Pergamon

Int. J. Solids Structures Vol. 31, No. 12/13, pp. 1635–1656, 1994
Elsevier Science Ltd
Printed in Great Britain
0020-7683/94 $7.00 + .00

0020-7683(93)E0016-B

DEVELOPMENT OF BEM FOR THERMOPLASTICITY

M. B. CHOPRA and G. F. DARGUSH
Department of Civil Engineering, State University of New York at Buffalo, Amherst, NY 14260, U.S.A.

Abstract—A boundary element method (BEM) for general thermoplastic analysis is presented. A thermally-sensitive two surface material model is used to simulate constitutive behavior. The nonlinear system of equations, arising from an initial stress approach, is solved using a new Newton–Raphson solution algorithm. The stress tensors are collapsed into a scalar variable using certain characteristic tensors arising out of the constitutive equations. This leads to a simpler system requiring much less computation. The solution algorithm is iterative in nature and checks for convergence at the end of each increment. The resulting robust analysis tool is then utilized in solving several practical applications to illustrate the growing importance of BEM as an alternative to the finite element method.

INTRODUCTION

The proper design of many critical components in the aerospace, automotive and nuclear industries depends upon accurate and timely thermoplastic analyses. While finite element method (FEM) formulations and computer codes already exist, it is beneficial to have alternative methodologies for such complex problems in order to verify results. In particular, analysis based upon the boundary element method (BEM) is potentially very attractive due to its ability to produce accurate solutions. The steep thermal and stress gradients, which are often present in thermomechanical problems, can be captured even with a fairly coarse BEM mesh (Dargush and Banerjee, 1989, 1990). Additionally, plasticity problems have been solved via BEM formulations with a high degree of accuracy by employing only a limited number of volume cells (e.g. Henry and Banerjee, 1988).

A preliminary BEM for thermoplastic analysis was presented in Dargush and Banerjee (1991) based upon a von Mises constitutive model and a nonlinear solution algorithm involving direct iteration. While that work contains the development of an appropriate integral formulation and kernel functions, the robustness of the overall algorithm was not sufficient for practical thermoplastic analyses. The present work represents an extension, which includes a more suitable material model and a more advanced solution procedure. As a result, the BEM presented here is applicable to a much broader range of thermoplastic problems.

The following sections provide details of the thermally-sensitive constitutive model, the integral formulation, and the Newton–Raphson solution algorithm employed in the current BEM. Afterward, several numerical applications are presented to highlight the effectiveness of the approach.

THERMALLY-SENSITIVE TWO-SURFACE MATERIAL MODEL

A temperature-dependent von Mises model was developed by Boley and Weiner (1960) for elastic–perfectly plastic material. Subsequently, Dargush and Banerjee (1991) made use of some of the concepts of soil mechanics along with the above mentioned work to put forth an isotropic hardening, temperature-dependent von Mises criterion. The yield strength of the material became a function of its temperature and was made to parabolically decay as the melting point was approached. However, this isotropic hardening von Mises model is based upon distinctly defined elastic and elastoplastic behavior and is inadequate in representing the smooth transition from elastic to a fully plastic state. Such a smooth behavior is usually observed in experiments conducted on metals and soils under cyclic loading conditions. A number of more advanced models were proposed in literature based

on the original work on nested yield surfaces by Mröz (1967). One such practical two-surface model was developed by Dafalias and Popov (1974) and Krieg (1975). It takes into account both kinematic and isotropic hardening behaviors and allows a smooth transition of states. A modified version of this model was subsequently proposed by Banerjee *et al.* (1987) which forms the basis of the present development. The present work marks the first implementation of a temperature dependent two-surface model within BEM.

This model assumes the existence of two yield surfaces in stress space, i.e. the inner or loading surface and the outer bounding surface. During loading, the stress point behaves in an elastic manner until it reaches the inner yield surface. The stress state then remains in contact with this inner surface, which translates in stress space in a manner described below. Once the inner yield surface touches the bounding surface, the behavior is then governed by an isotropic hardening rule for the outer surface. Subsequent plastic deformation results in the isotropic expansion of the outer surface and simultaneous translation of the inner surface to remain in contact with the outer. Thus, all transitions in the stiffness states of the material are carried out in a smooth manner. The yield functions associated with the loading and bounding surfaces are assumed to have the same shape and orientation and are defined by thermally-sensitive von Mises models (Dargush and Banerjee, 1991). Using an associated flow rule and the consistency conditions, the governing constitutive relationship may be derived as follows:

$$\dot{\sigma}_{ij} = D^e_{ijkl}\dot{\varepsilon}^m_{kl} - D^e_{ijkl}\left(\frac{\partial f}{\partial \sigma_{kl}}\right)\left[\frac{\left(\frac{\partial f}{\partial \sigma_{mn}}\right)D^e_{mnpq}\dot{\varepsilon}^m_{pq} + \left(\frac{\partial f}{\partial T}\right)\dot{T}}{H^e + H^p}\right], \tag{1a}$$

where

$$H^e = \left(\frac{\partial f}{\partial \sigma^b_{ij}}\right) D^e_{ijkl}\left(\frac{\partial f}{\partial \sigma^b_{kl}}\right). \tag{1b}$$

D^e_{ijkl} is the elastic constitutive tensor, f is the yield function, σ_{ij} is the stress state on the loading surface, σ^b_{ij} is the stress state on the bounding surface, $\dot{\varepsilon}^m_{ij}$ is the incremental mechanical strain, $\dot{T}$ is the incremental temperature from some reference value and H^p is the plastic hardening modulus. H^p is determined from the position of the stress state relative to the loading and bounding surfaces and the hardening associated with the bounding surface as:

$$H^p = h^b\left[\frac{\bar{\beta}}{\sigma^b_y}\right]^n, \tag{2}$$

where

h^b = hardening parameter associated with the bounding surface,
$\bar{\beta} = [\beta_{ij}\beta_{ij}]^{1/2}$,
β_{ij} = the stress vector connecting the current stress state to the last location of the loading surface center when the material was elastic,
σ^b_y = equivalent stress state on the bounding surface = $[\sigma^b_{ij}\sigma^b_{ij}]^{1/2}$,
n = specified power parameter,
σ_y = equivalent stress state on the loading surface.

The hardening parameter associated with both surfaces is thermally sensitive. Further details of this model may be found in Chopra (1991).

INTEGRAL FORMULATION

This section is devoted to the development of integral equations for temperatures, displacements and stresses for thermoplasticity. An initial stress approach is utilized for incremental plasticity (Banerjee and Butterfield, 1981), where the initial stress increment is defined as:

$$\dot{\sigma}^{o}_{ij} = \dot{\sigma}^{e}_{ij} - \dot{\sigma}_{ij}, \tag{3}$$

in which $\dot{\sigma}^{e}_{ij}$ is the elastic stress increment and $\dot{\sigma}_{ij}$ is the elastoplastic stress increment.

The conventional boundary integral equation in three-dimensions for generalized displacements (i.e. displacements and temperature) is extended to the domain of nonlinear analysis by incorporating the effects of the volume integral terms as follows (Dargush and Banerjee, 1991):

$$c_{\beta\alpha}(\xi)\dot{u}_{\beta}(\xi,\tau) = \int_S [G_{\beta\alpha}(X;\xi,\tau)\dot{t}_{\beta}(X,\tau) - F_{\beta\alpha}(X;\xi,\tau)\dot{u}_{\beta}(X,\tau)]\,\mathrm{d}S(X)$$

$$+ \int_S [g^{tr}_{T\alpha}(X;\xi,\tau) * \dot{t}_T(X) - f^{tr}_{T\alpha}(X;\xi,\tau) * \dot{u}_T(X)]\,\mathrm{d}S(X) + \int_V [B_{ik\alpha}(X;\xi,\tau)\dot{\sigma}^{o}_{ik}(X,\tau)]\,\mathrm{d}V(X)$$

$$+ \int_V [G_{T\alpha}(X;\xi,\tau)\dot{\psi}^{o}(X,\tau) + g^{tr}_{T\alpha}(X;\xi,\tau) * \dot{\psi}^{o}(X)]\,\mathrm{d}V(X), \tag{4}$$

where $\dot{u}_{\beta}$ are the generalized incremental displacements, $\dot{t}_{\beta}$ are the generalized incremental tractions, $G_{\beta\alpha}$, $F_{\beta\alpha}$ are the steady-state portions of displacement kernels while $g^{tr}_{T\alpha}$ and $f^{tr}_{T\alpha}$ are the transient thermal portions, respectively. For three-dimensional domains, the lower case Latin indices assume the values 1, 2 and 3, the Greek indices vary from 1 to 4, while the subscript T represents 4. Furthermore,

$$\dot{\psi}^{o}(X,\tau) = \gamma\sigma_{ij}\dot{\varepsilon}^{p}_{ij},$$

with γ as a non-dimensional material parameter indicating the fraction of the total inelastic dissipation that is converted into heat. The volume kernel $B_{ik\alpha}$ is constructed from $G_{j\alpha}$ by using the following relationship

$$B_{ik\alpha} = \frac{1}{2}\left[\frac{\partial G_{i\alpha}}{\partial x_k} + \frac{\partial G_{k\alpha}}{\partial x_i}\right]. \tag{5}$$

As seen from (4), the complete kernels are decomposed into steady-state and transient parts. All the singularities are contained in the steady part, while the transient part is completely nonsingular. All boundary kernels are identical to those for the linear case.

The kernel B_{ikj} is identical to static elastoplasticity and can be found explicitly in Henry and Banerjee (1988). The last row in $B_{ik\alpha}$ corresponding to the temperature is completely zero. Detailed expressions for all kernels are available in Dargush and Banerjee (1991) and Chopra (1991).

By utilizing the strain–displacement relationship along with the constitutive law, the integral equation for stress rate in the interior of body, becomes

$$\dot{\sigma}_{ij}(\xi,\tau) = \int_S [G^{\sigma}_{\beta ij}\dot{t}_{\beta} - F^{\sigma}_{\beta ij}\dot{u}_{\beta}]\,\mathrm{d}S + \int_V [B^{\sigma}_{klij}\dot{\sigma}^{o}_{kl} + G^{\sigma}_{Tij}\dot{\psi}^{o})\,\mathrm{d}V$$

$$+ \int_S [{}^{tr}g^{\sigma}_{Tij} * \dot{t}_T - {}^{tr}f^{\sigma}_{Tij} * \dot{u}_T]\,\mathrm{d}S + \int_V [{}^{tr}g^{\sigma}_{Tij} * \dot{\psi}^{o}]\,\mathrm{d}V + J^{\sigma}_{klij}\dot{\sigma}^{o}_{kl}, \tag{6}$$

where the kernels $G^{\sigma}_{\beta ij}$ and $F^{\sigma}_{\beta ij}$ are the steady thermoelastic stress kernels, while J^{σ}_{klij} represents the standard plasticity jump terms. The volume kernel for the stress equation are described by

$$B^{\sigma}_{klij} = \frac{2\mu\nu}{1-2\nu}\delta_{ij}\frac{\partial B_{klm}}{\partial \xi_m} + \mu\left(\frac{\partial B_{kli}}{\partial \xi_j} + \frac{\partial B_{klj}}{\partial \xi_i}\right) - \beta\delta_{ij}B_{klT}. \tag{7}$$

The initial stress kernel B^{σ}_{klij} has a strong singularity and the corresponding volume integral needs special attention as discussed later.

At this juncture, some characteristic relationships arising out of the development of constitutive models are discussed. It was observed by Banerjee and Raveendra (1987) that a scalar quantity $\dot{\lambda}$ can be introduced to greatly reduce the computational burden associated with BEM for elastoplastic analysis. Extending this concept to the thermoplastic case, the following identities hold:

$$\dot{\lambda} = L^{\sigma}_{ij}\dot{\sigma}_{ij} + L^{T}\dot{T}, \tag{8a}$$

$$\dot{\sigma}^{o}_{ij} = K_{ij}\dot{\lambda}. \tag{8b}$$

From (8b), it is clear that the unknown initial stress tensor may be collapsed into a scalar unknown $\dot{\lambda}$, by using the tensor K_{ij}. Furthermore, the integral equation for stress rates can be collapsed from a set of equations for each stress component into a single equation for the unknown scalar $\dot{\lambda}$ using (8a). As a result, the initial stress rates, $\dot{\sigma}^{o}_{ij}$, appearing in the two integral equations, namely (4) and (6), can be replaced by $\dot{\lambda}$. Thus:

$$c_{\beta\alpha}(\xi)\dot{u}_{\beta}(\xi,\tau) = \int_S [G_{\beta\alpha}\dot{t}_{\beta} - F_{\beta\alpha}\dot{u}_{\beta}]\,\mathrm{d}S + \int_V [B_{ik\alpha}K_{ik}\dot{\lambda} + G_{T\alpha}\dot{\psi}^{o}]\,\mathrm{d}V$$
$$+ \int_S [g^{tr}_{T\alpha} * \dot{t}_T - f^{tr}_{T\alpha} * \dot{u}_T]\,\mathrm{d}S + \int_V [g^{tr}_{T\alpha} * \dot{\psi}^{o}]\,\mathrm{d}V \tag{9}$$

and the incremental stress equation (6) becomes

$$\dot{\lambda}(\xi,\tau) = L^{\sigma}_{ij}(\xi)\left\{\int_S [G^{\sigma}_{\beta ij}\dot{t}_{\beta} - F^{\sigma}_{\beta ij}\dot{u}_{\beta}]\,\mathrm{d}S + \int_V [B^{\sigma}_{klij}K_{kl}\dot{\lambda} + G^{\sigma}_{Tij}\dot{\psi}^{o}]\,\mathrm{d}V\right.$$
$$\left. + \int_S [{}^{tr}g^{\sigma}_{Tij} * \dot{t}_T - {}^{tr}f^{\sigma}_{Tij} * \dot{u}_T]\,\mathrm{d}S + \int_V [{}^{tr}g^{\sigma}_{Tij} * \dot{\psi}^{o}]\,\mathrm{d}V + J^{\sigma}_{klij}K_{kl}\dot{\lambda}\right\} + L^{T}\dot{T}. \tag{10}$$

Equations (9) and (10) are utilized together in solving the unknown increments of generalized boundary quantities along with the scalar $\dot{\lambda}$ for the interior unknowns. With this approach, $\dot{\lambda}$ is used as a primary unknown and introduced into an iterative scheme. The initial stress rates are then computed from $\dot{\lambda}$ within this scheme. It may be pointed out at this stage that the characteristic tensors K_{ij} and L^{σ}_{ij}, along with the scalar L^{T}, are functions of the current stress state and do not depend upon any incremental quantities.

The integral equations expressed by (9) and (10) are exact statements. However, in order to utilize these for solving realistic problems with complex geometries and multiple time steps, a temporal and spatial discretization of these equations becomes necessary. The discretization in time is carried out using standard time-marching techniques outlined in Dargush and Banerjee (1991). The time interval between zero and current time t is divided into N equal increments of duration Δt. The primary variables in the integral equation must be handled in a rate form and an approximation is made by assuming that the variables, $\dot{u}_{\beta}$, $\dot{t}_{\beta}$ and $\dot{\lambda}$ remain constant within each time increment.

The evaluation of the surface integrals requires the discretization of the boundary. Spatial discretization techniques have been discussed in previous references and are not

repeated here. However, it must be noted that, for the nonlinear case of thermoplasticity, the volume integrals appearing in the integral equations require additional domain discretization. Typically, the potentially plastic regions are localized to a small zone occupying only a part of the entire body. Volume cells are confined to those regions.

The strongly singular nature of the volume kernel B^{σ}_{klij} is handled using an indirect method known as the initial stress expansion technique (Henry and Banerjee, 1988). All the remaining steady-state volume kernels are, at worst, weakly singular in nature. For the weakly singular kernels, a Gaussian quadrature numerical scheme is utilized. Subsegmentation and higher order adaptive quadrature rules are used in error control in a manner similar to the surface integral evaluations. Further details of the schemes for evaluating the volume integrals may be found in Mustoe (1984) and Banerjee and Raveendra (1986).

The assembly process using the collocation method proceeds along the lines of the linear case with additional collocation for the volume nodes. The coefficients from the boundary equation for each boundary node and from the interior equation for each volume node are assembled to arrive at the final system of equations. The next step is to collect the known and unknown values of the primary surface variables from the specified boundary conditions. At common interfaces of substructured regions, the equilibrium and compatibility conditions are invoked in a manner described in Banerjee and Butterfield (1981).

The system of equations is now ready for solution and may be rephrased in matrix (bold letters) notation as

$$\mathbf{A}^{b}\dot{\mathbf{x}}^{N} = \dot{\mathbf{b}}^{N} + \mathbf{C}^{b}\mathbf{K}\dot{\lambda}^{N} \tag{11a}$$

$$\dot{\lambda}^{N} = -\mathbf{L}^{\sigma}\mathbf{A}^{\sigma}\dot{\mathbf{x}}^{N} + \mathbf{L}^{\sigma}\dot{\mathbf{b}}^{\sigma N} + \mathbf{L}^{\sigma}\mathbf{C}^{\sigma}\mathbf{K}\dot{\lambda}^{N}. \tag{11b}$$

The matrices $\mathbf{A}^{b}$ and $\mathbf{A}^{\sigma}$ are block banded while $\mathbf{C}^{b}$ and $\mathbf{C}^{\sigma}$ are block diagonal through the assembly process. The vectors $\dot{\mathbf{b}}^{N}$ and $\dot{\mathbf{b}}^{\sigma N}$ contain the effects of all known quantities, including the contribution from previous time steps. These equations cannot be solved directly since $\mathbf{L}^{\sigma}$ and $\mathbf{K}$ are themselves unknown and an iterative algorithm must be used for this purpose. A new Newton–Raphson solution algorithm has been developed as a part of the present work.

NEWTON–RAPHSON SOLUTION ALGORITHM

The system equations (11) are rearranged in the form of residue (or error) terms for the Nth time step as follows:

$$\mathbf{g}^{b}(\dot{\mathbf{x}}, \dot{\lambda}) = \mathbf{A}^{b}\dot{\mathbf{x}} - \dot{\mathbf{b}} - \mathbf{C}^{b}\mathbf{K}\dot{\lambda} = 0, \tag{12a}$$

$$\mathbf{g}^{\lambda}(\dot{\mathbf{x}}, \dot{\lambda}) = \mathbf{L}^{\sigma}\mathbf{A}^{\sigma}\dot{\mathbf{x}} - \mathbf{L}^{\sigma}\dot{\mathbf{b}}^{\sigma} - \mathbf{L}^{\sigma}\mathbf{C}^{\sigma}\mathbf{K}\dot{\lambda} + \mathbf{I}\dot{\lambda} = 0. \tag{12b}$$

An iterative scheme is developed wherein the error functions $\mathbf{g}^{b}$ and $\mathbf{g}^{\lambda}$ are minimized. Writing the Taylor series expansion for $\mathbf{g}^{b}(\dot{\mathbf{x}}, \dot{\lambda})$ with respect to $\dot{\mathbf{x}}$ and $\dot{\lambda}$ for the mth iteration, produces:

$$\mathbf{g}^{b}(\dot{\mathbf{x}}, \dot{\lambda}) = \mathbf{g}^{b}(\dot{\mathbf{x}}^{m}, \dot{\lambda}^{m}) + \frac{\partial \mathbf{g}^{b}}{\partial \dot{\mathbf{x}}}(\Delta\dot{\mathbf{x}}^{m}) + \frac{\partial \mathbf{g}^{b}}{\partial \dot{\lambda}}(\Delta\dot{\lambda}^{m}) + \text{higher order terms} \ldots = 0, \tag{13a}$$

$$\mathbf{g}^{\lambda}(\dot{\mathbf{x}}, \dot{\lambda}) = \mathbf{g}^{\lambda}(\dot{\mathbf{x}}^{m}, \dot{\lambda}^{m}) + \frac{\partial \mathbf{g}^{\lambda}}{\partial \dot{\mathbf{x}}}(\Delta\dot{\mathbf{x}}^{m}) + \frac{\partial \mathbf{g}^{\lambda}}{\partial \dot{\lambda}}(\Delta\dot{\lambda}^{m}) + \text{higher order terms} \ldots = 0, \tag{13b}$$

where $(\Delta\dot{\mathbf{x}}^{m})$ and $(\Delta\dot{\lambda}^{m})$ are the changes in the incremental quantities during the mth iteration of the current load increment. The quantities $\dot{\mathbf{x}}^{m}$ and $\dot{\lambda}^{m}$ are the values of $\dot{\mathbf{x}}$ and $\dot{\lambda}$ computed at the end of the $(m-1)$th increment. Therefore, $\dot{\mathbf{x}}^{m}$ and $\dot{\lambda}^{m}$ are known quantities for the mth iteration. Neglecting the higher order terms and rearranging, equation (13) yields the following system equation:

$$\begin{bmatrix} \dfrac{\partial \mathbf{g}^b}{\partial \dot{\mathbf{x}}} & \dfrac{\partial \mathbf{g}^b}{\partial \dot{\lambda}} \\ \dfrac{\partial \mathbf{g}^\lambda}{\partial \dot{\mathbf{x}}} & \dfrac{\partial \mathbf{g}^\lambda}{\partial \dot{\lambda}} \end{bmatrix} \begin{Bmatrix} (\Delta \dot{\mathbf{x}}^m) \\ (\Delta \dot{\lambda}^m) \end{Bmatrix} = \begin{Bmatrix} -\mathbf{g}^b(\dot{\mathbf{x}}^m, \dot{\lambda}^m) \\ -\mathbf{g}^\lambda(\dot{\mathbf{x}}^m, \dot{\lambda}^m) \end{Bmatrix}. \tag{14}$$

Each partial derivative term is evaluated and the final form of equation (14) may be written explicitly as

$$\begin{bmatrix} \mathbf{A}^b & -\mathbf{C}^b\mathbf{K} \\ \mathbf{L}^\sigma\mathbf{A}^\sigma & \mathbf{I}-\mathbf{L}^\sigma\mathbf{C}^\sigma\mathbf{K} \end{bmatrix} \begin{Bmatrix} (\Delta \dot{\mathbf{x}}^m) \\ (\Delta \dot{\lambda}^m) \end{Bmatrix} = \begin{Bmatrix} -(\mathbf{A}^b\dot{\mathbf{x}}^m - \dot{\mathbf{b}} - \mathbf{C}^b\mathbf{K}\dot{\lambda}^m) \\ -(\mathbf{L}^\sigma\mathbf{A}^\sigma\dot{\mathbf{x}}^m - \mathbf{L}^\sigma\dot{\mathbf{b}}^\sigma - \mathbf{L}^\sigma\mathbf{C}^\sigma\mathbf{K}\dot{\lambda}^m + \mathbf{I}\dot{\lambda}^m) \end{Bmatrix}. \tag{15}$$

Further, in a global matrix form this becomes simply:

$$[\mathbf{A}^G]\{\Delta \dot{\mathbf{X}}^m\} = \{\mathbf{R}^m\}, \tag{16}$$

where $[\mathbf{A}^G]$ is the system matrix, $\{\Delta \dot{\mathbf{X}}^m\}$ is a matrix of the generalized unknowns comprising of $\Delta\dot{\mathbf{x}}$, $\Delta\dot{\lambda}$ and $\{\mathbf{R}^m\}$ is the entire right-hand side vector for the mth iteration. For certain problems, the system matrix $\mathbf{A}^G$ may not be required to be recomputed for each iteration. This corresponds to the case of a Modified Newton–Raphson scheme wherein the system matrix is only reassembled after a prescribed number of iterations.

It may be mentioned here that the variable stiffness method proposed by Banerjee and Raveendra (1987) forms a special case of the more general Newton–Raphson schemes presented above. In particular, the variable stiffness algorithm is recovered from (15), if the number of iterations is fixed at one and the equations are solved by first inverting $(\mathbf{I}-\mathbf{L}^\sigma\mathbf{C}^\sigma\mathbf{K})$ and then backsubstituting for $\Delta\dot{\lambda}$.

The entire iterative scheme used to solve eqn (16) is illustrated through the flowchart shown in Fig. 1. A detailed description of the algorithm is provided in Chopra (1991). The nonlinear BEM formulation with the Newton–Raphson algorithm described above, is implemented in a general purpose BEM computer program (GPBEST). Consequently, all the features of the large scale, state-of-the-art code can be directly utilized for the present analysis.

NUMERICAL APPLICATIONS

(1) *Residual stress in a steel cylinder*

As the first application of quasistatic thermoplasticity, consider the residual stresses resulting from the sudden cooling of a steel cylinder. The cylinder is long and has a diameter of 2.5 in. It is initially at a temperature of 1250°F without any stresses and is subsequently cooled in an 80°F fluid. The rate of convection is governed by the film coefficient specified along its cylindrical surface. A film coefficient of $h = 12.24\ \text{in}-\text{lb}(\text{s in}^2\ ^\circ\text{F})^{-1}$ is selected to simulate a fairly rapid cooling process.

The material properties, corresponding to 1060 Steel, are selected as

$$E = 30\times10^6\ \text{psi} \qquad k = 5.8\ \text{in}-\text{lb}(\text{s in}\ ^\circ\text{F})^{-1}$$
$$\nu = 0.3 \qquad \rho c_\varepsilon = 283.0\ \text{in}-\text{lb}(\text{in}^3\ ^\circ\text{F})^{-1}$$
$$\alpha = 6.0\times10^{-6}\ (^\circ\text{F})^{-1}.$$

In addition, a thermally-sensitive von Mises constitutive model is employed with the yield stress at reference temperature, $\sigma_y = 48$ ksi, and the melting temperature, $T_{\text{melt}} = 1300$°F. No strain-hardening is permitted to take place.

The axisymmetric BEM mesh utilized for this problem is shown in Fig. 2(a) and consists of six quadratic boundary elements and four quadratic volume cells. For constructing the eight-noded cells, eight additional nodes within the volume are required, including some on the axis of symmetry. However, the axis of symmetry is not modeled with boundary

elements. A time step size of 4.0 s was found suitable for this problem, based upon the smallest significant element length as well as the diffusivity. This step size was further confirmed through convergence studies. In addition to the mesh described above, a more refined mesh with 16 volume cells was also constructed to verify the convergence of the results obtained from the present analysis. This finer mesh is displayed in Fig. 2(b).

The temperature response, as a function of time at the surface ($r = 1.25$) and at the center ($r = 0.0$) of the cylinder at midheight, is shown in Fig. 3(a). A rapid cooling takes place at the surface, as expected, whereas the center cools more gradually. After about 80 s, the entire cylinder is close to room temperature and the analysis is terminated. The sudden cooling phenomenon gives rise to differential stress behavior in the cylinder, as evident from

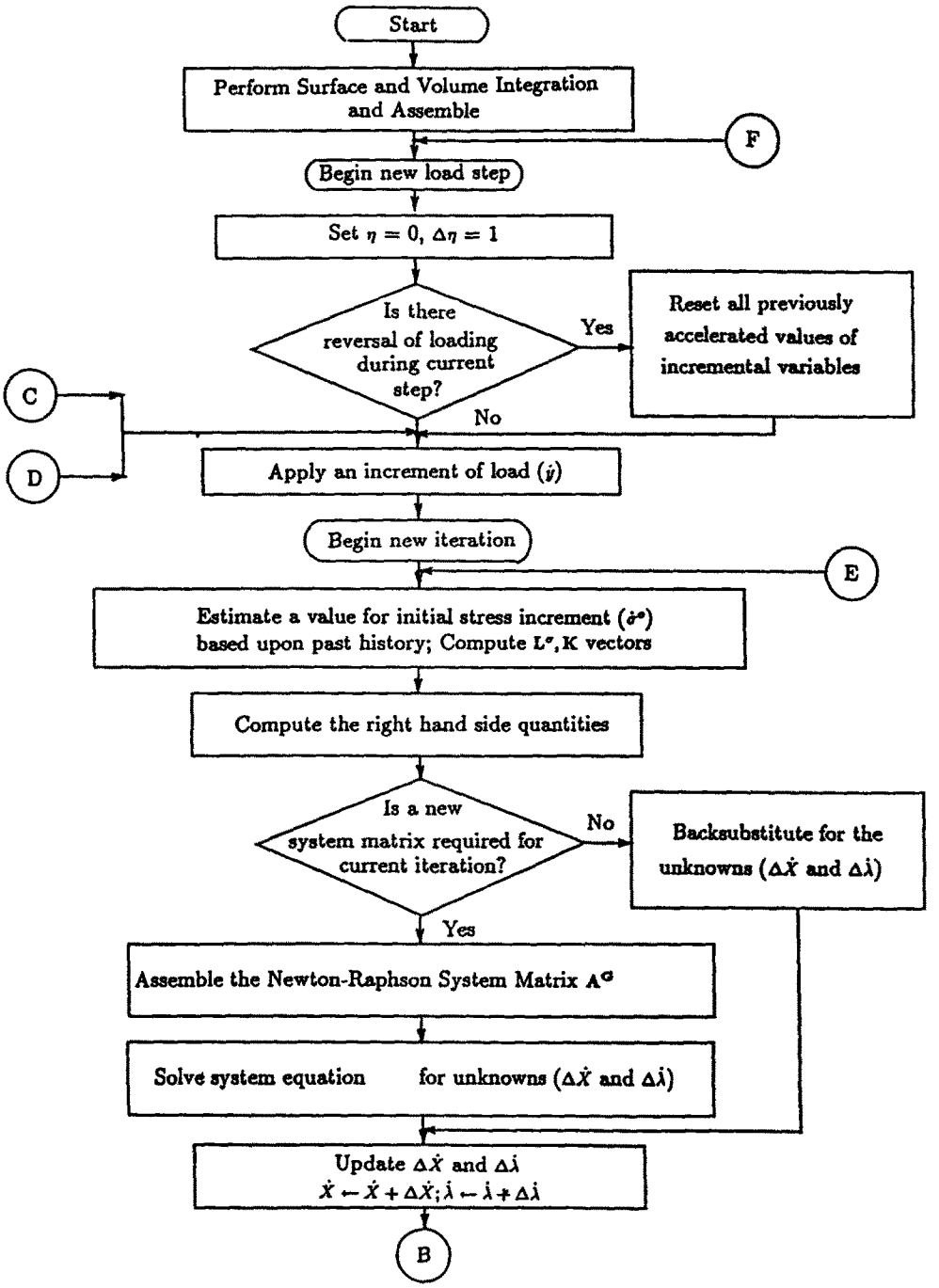

Fig. 1. Flowchart describing the Newton–Raphson iterative solution algorithm.

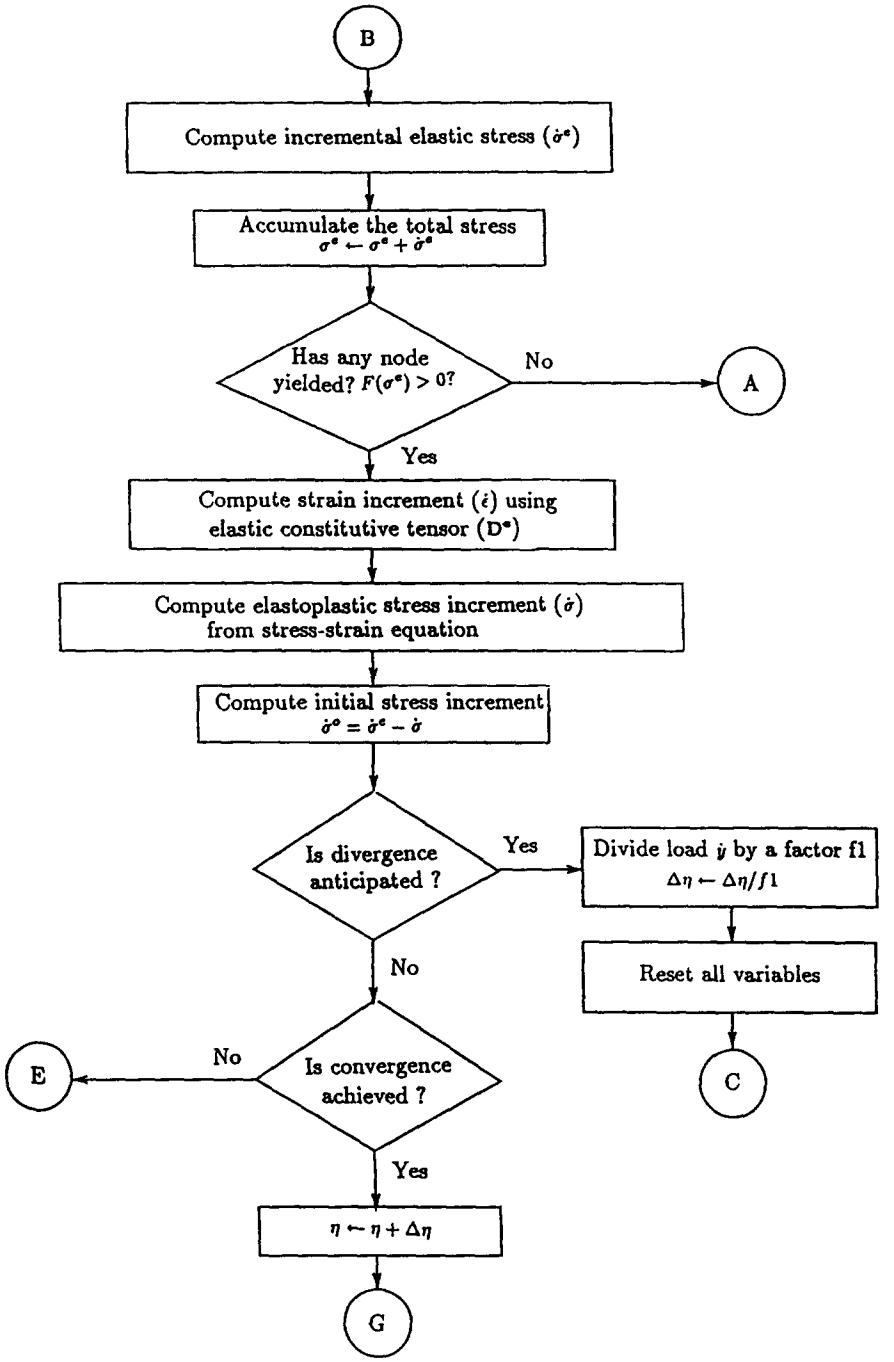

Fig. 1.—*Continued.*

Fig. 3(b). The axial stresses are plotted at the same locations (i.e. $r = 0.0$ and 1.25) showing the variation with time. The surface of the cylinder develops tensile stress initially, while the center goes into compression. However, since the material is still very hot, yielding commences at a much lower value of stress and considerable plastic flow results. Eventually, after the first 10 s, the thermal gradients diminish and the current yield stress value increases, reducing the amount of plastic flow. The behavior is altered as a result, and elastic unloading begins to occur. Ultimately, after about 40.0 s, the surface goes into compression whereas the stress at the center diminishes in value. At the stage where the analysis is terminated, the cylinder exhibits a compressive stress of 40.0 ksi at the surface while the center has a small amount of tensile stress.

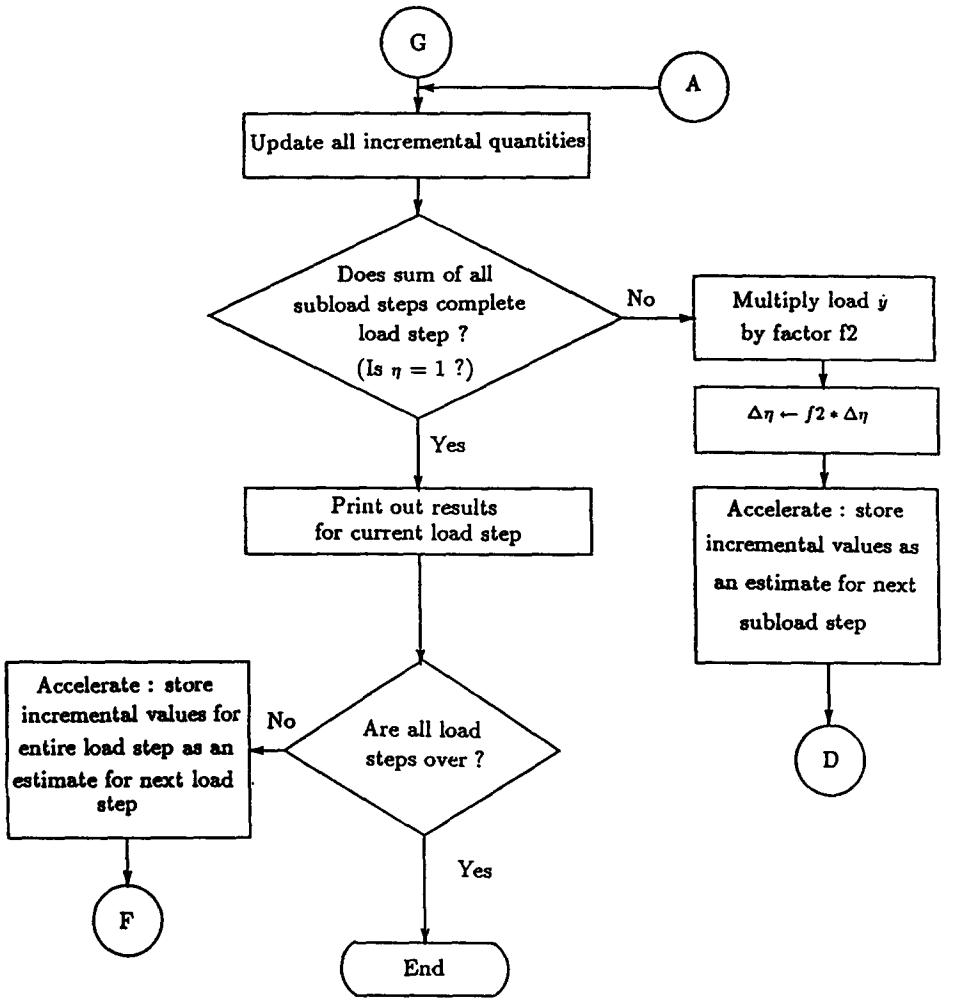

Fig. 1.—*Continued.*

Next, an important aspect of this problem is investigated in more detail. The effect of the rate of convection embodied in the film coefficient, on the stress behavior is studied. Three values of h, namely $h = 1.224$, 12.24 and 122.4 in−lb(s in^2 °F)$^{-1}$, are selected in order to simulate slow, intermediately rapid and very rapid cooling, respectively. This becomes evident from the plots of the temperature behavior with time for the three h values at the center [Fig. 4(a)] as well as the surface [Fig. 4(b)]. The axial stress variation with time for the three cases is shown in Fig. 5(a) for $r = 0.0$ and Fig. 5(b) for $r = 1.25$ in. As expected, the slow cooling case depicts very little stress build-up with time and consequently, very little residual stress. On the opposite end, the very rapid cooling case shows an initial build-up of stress followed by unloading, at both locations. This case also exhibits a much higher residual tensile stress at the center in comparison to the intermediate case.

(2) *Pressure vessel containing a hot fluid*

The next application studied is the thermoplastic analysis of an axisymmetric, steel pressure vessel subjected to internal pressure of a fluid at a high temperature. The combined effect of the mechanical and thermal loading produces a complex stress pattern within the walls of the vessel. Assuming the material obeys an elastoplastic stress–strain law, the internal pressure of the fluid is sufficient to cause yielding, particularly around the welded connection between the shell and the neck. This elastoplastic behavior was studied by Zienkiewicz (1977) using FEM and by Henry and Banerjee (1988) using an elastoplastic BEM formulation. In addition, some experimental observations of the behavior of the

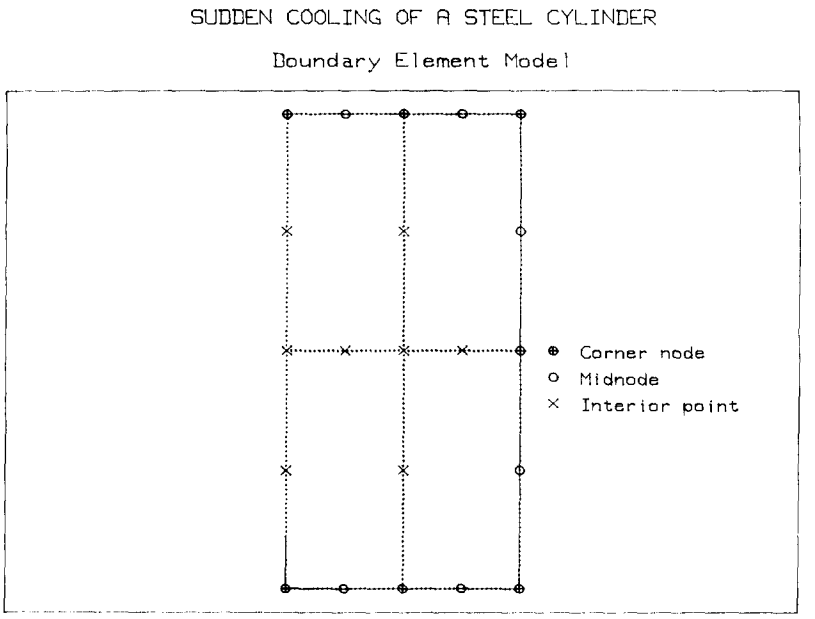

(a)

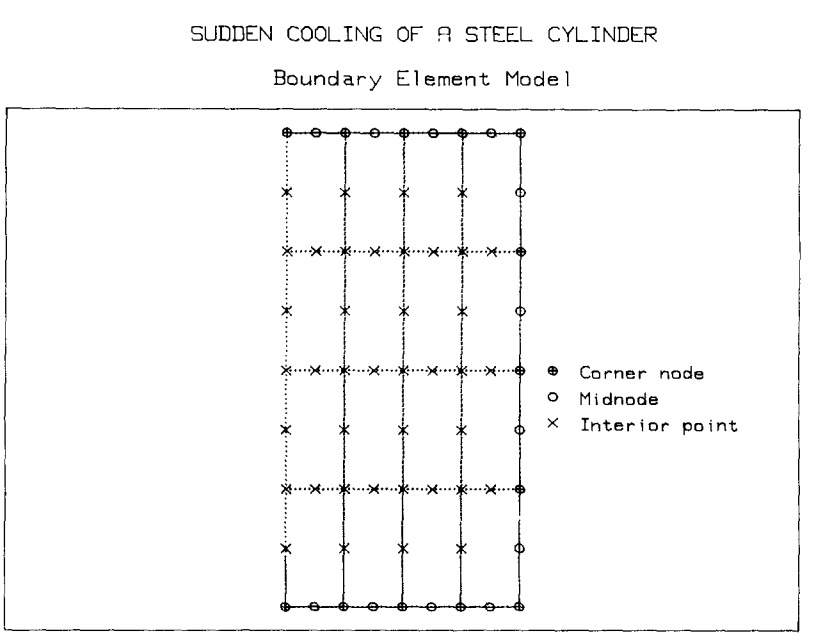

(b)

Fig. 2(a) Residual stress in a steel cylinder—boundary element model; (b) Residual stress in a steel cylinder—finer mesh.

vessel due to internal pressure have been presented by Dinno and Gill (1965). In the present analysis, the thermal effects are superimposed onto the elastoplastic mechanical analysis to study the combined response. The temperature of the fluid is related to the internal pressure on the wall by the following relationship:

$$P = AT^n$$

where $A = 37.947$ and $n = 0.5$. The problem description, along with the dimensions of the

(a)

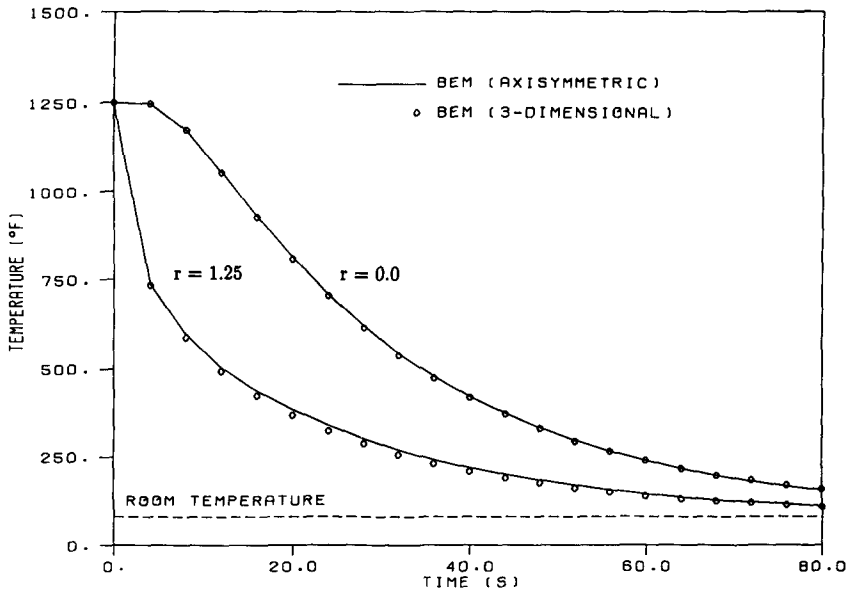

(b)

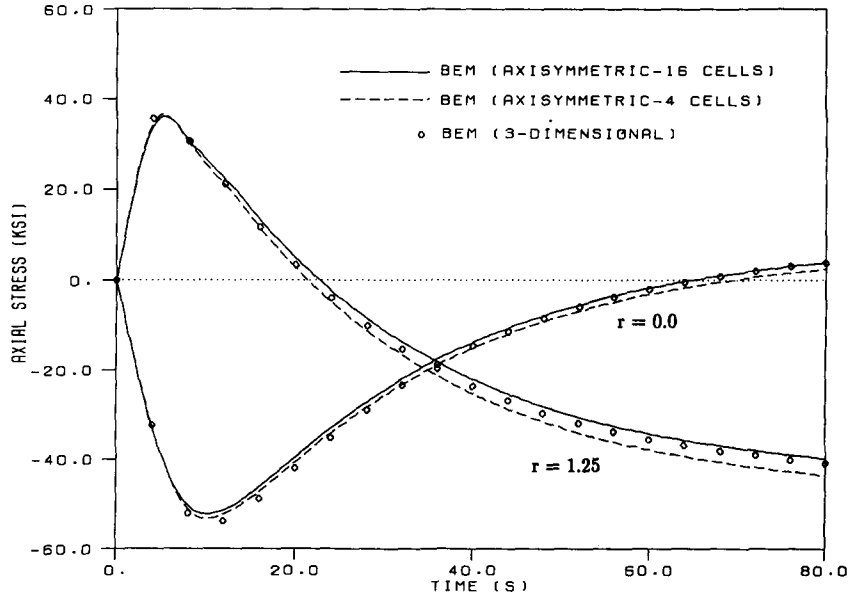

Fig. 3(a) Temperature variation with time at $r = 0$ (centerline) and $r = 1.25$ (surface); (b) Axial stress variation with time at $r = 0$ and $r = 1.25$.

vessel, is provided in Fig. 6(a). The pressure–temperature relation defined above is represented graphically in Fig. 6(b).

The vessel is made of steel and the following material properties apply:

$$E = 29.12 \times 10^6 \text{ psi}$$

$$\nu = 0.3$$

$$\alpha = 6.0 \times 10^{-6} \text{ in(in °F)}^{-1}$$

$$\rho c_\varepsilon = 283.0 \text{ in} - \text{lb(in}^3 \text{ °F)}^{-1}$$

$$k = 5.8 \text{ in} - \text{lb(s in °F)}^{-1}.$$

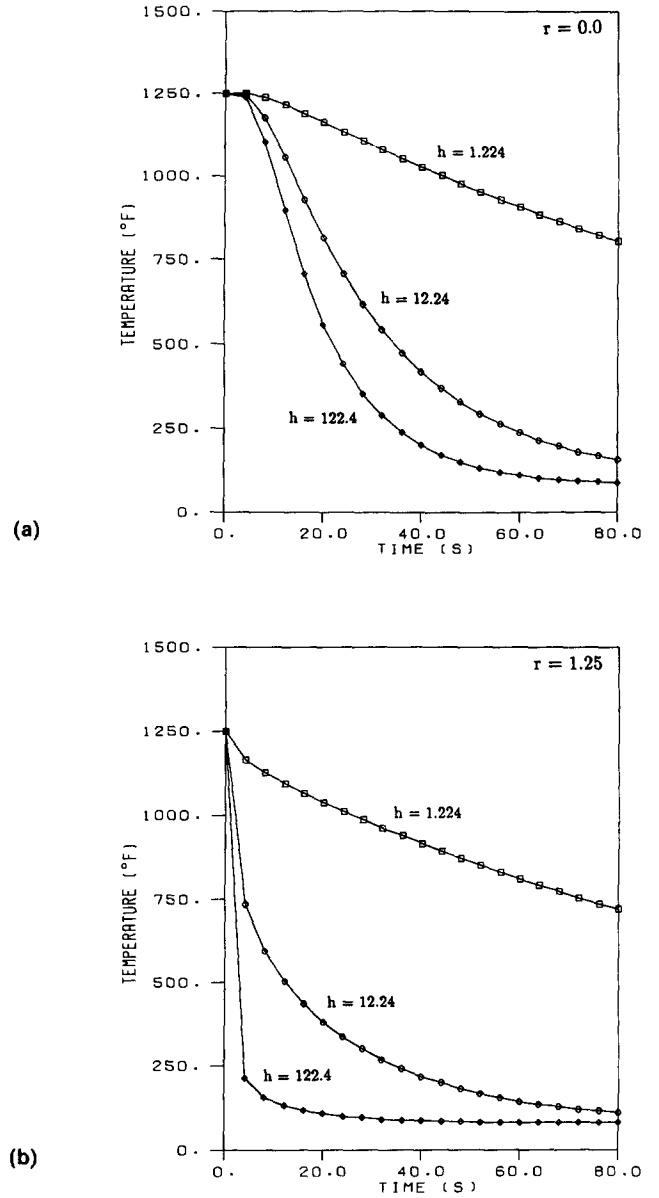

Fig. 4(a) Temperature variation with time at $r = 0$ for $h = 1.224$, 12.24 and 122.4; (b) Temperature variation with time at $r = 1.25$ for $h = 1.224$, 12.24 and 122.4.

The thermally-sensitive von Mises model is adopted with a yield stress at reference temperature of $\sigma_y = 40.54$ ksi and no strain-hardening. The melting temperature of steel is taken as $T_{\text{melt}} = 1400°\text{F}$. The temperature of the fluid within the vessel is taken as 410°F and the corresponding internal pressure is 700 psi. A more severe loading case is also modeled where the temperature of the fluid is raised to 632°F and the applied pressure becomes 900 psi. The outside environment of the vessel is maintained at 70°F.

A six region, axisymmetric BEM mesh, with 99 quadratic boundary elements and 12 volume cells, is employed to model the vessel, as depicted in Fig. 7. The volume cells are only placed in zones of potential yielding. Intuitively, the area around the welded connection would appear the likely zone for plasticity to occur. Hence, only region 4 is assumed to contain cells and all other regions are treated elastically. Of course, it must be verified at the completion of the analysis that, indeed, no plastic effects were present in these elastic regions.

First, an isothermal room temperature, steady-state analysis is conducted in order to

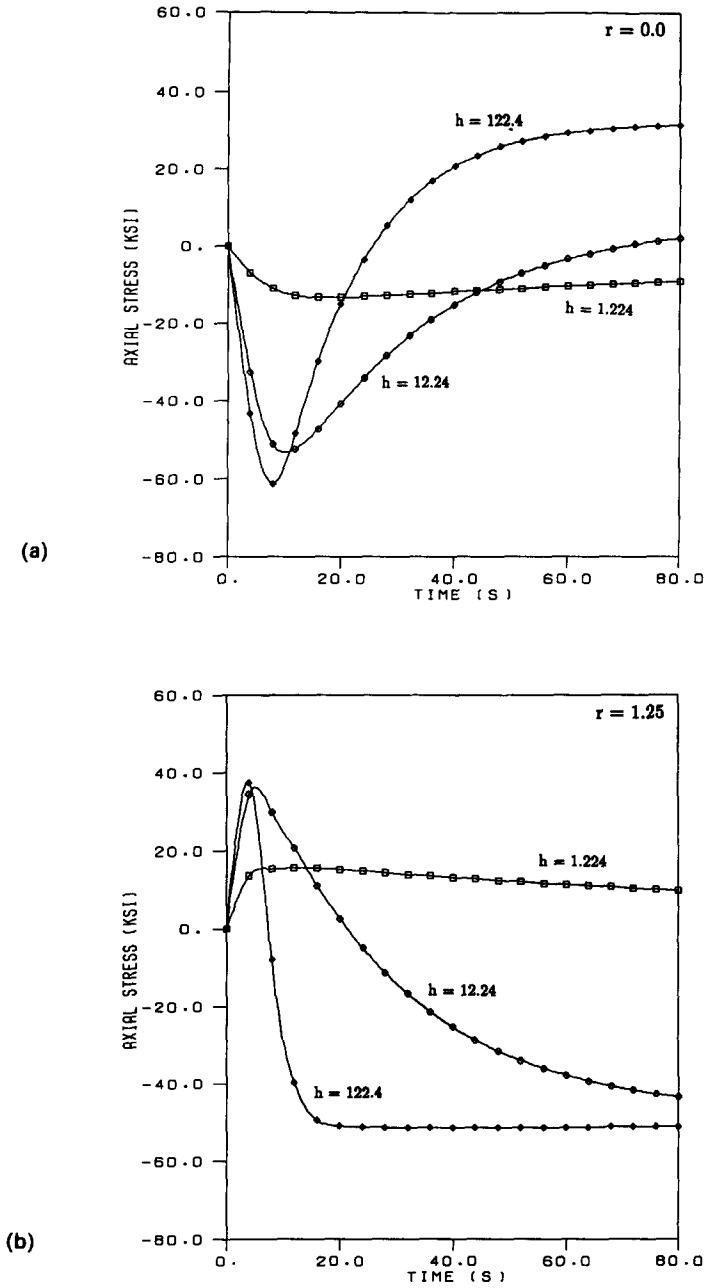

Fig. 5(a) Variation of axial stress with time at $r = 0$ for $h = 1.224$, 12.24 and 122.4; (b) Variation of axial stress with time at $r = 1.25$ for $h = 1.224$, 12.24 and 122.4.

simulate an elastoplastic analysis and compare with the known solutions mentioned above. The results of the present BEM analysis for the vertical deflection of point "A" as a function of the applied pressure are plotted in Fig. 8(a). Also plotted alongside are the FEM results of Zienkiewicz (1977) and the experimental results of Dinno and Gill (1965). The BEM results are observed to agree very well with the FEM results. However, both solutions differ slightly from the experimental results. This may be attributed to the choice of the von Mises model and the assumption of ideal plasticity. Furthermore, the entire body is considered to be homogeneous, whereas, in reality, the welded region would differ significantly in behavior. Nevertheless, the overall correlation appears very satisfactory and may be further improved by imparting some degree of strain hardening to the material. Figure 7(b) shows the progress of the yielded zones with increasing values of the internal pressure. The results

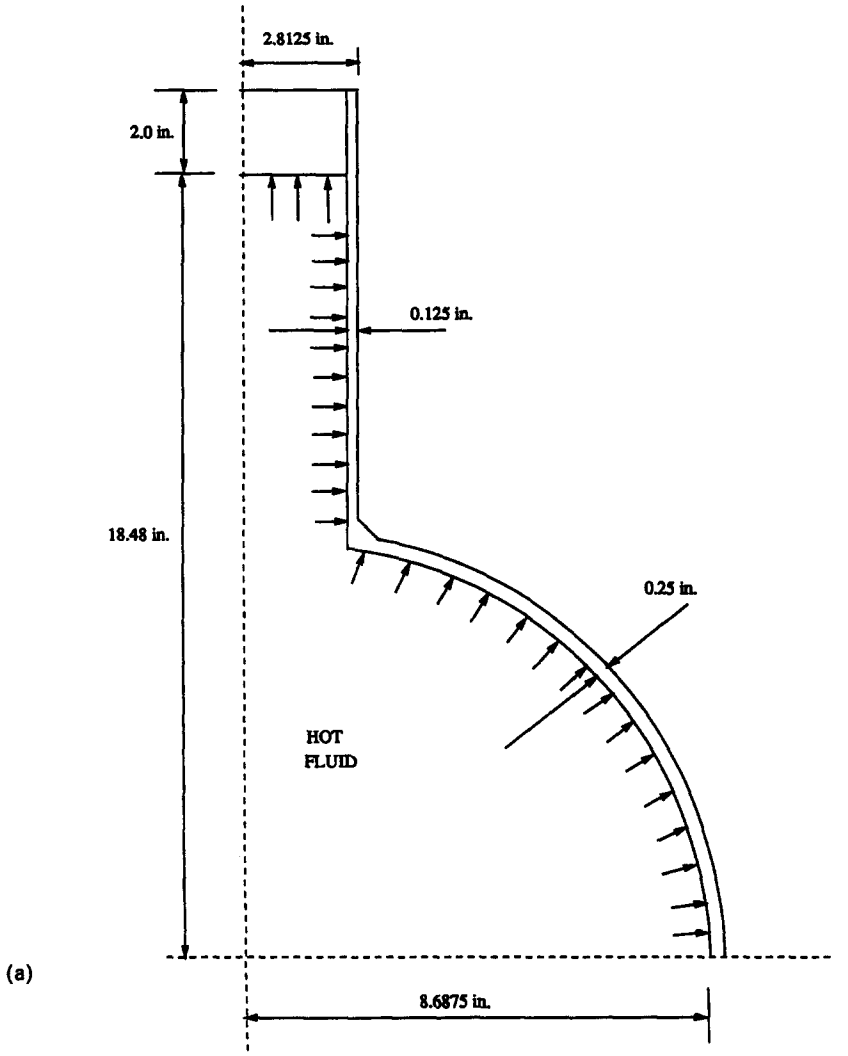

(a)

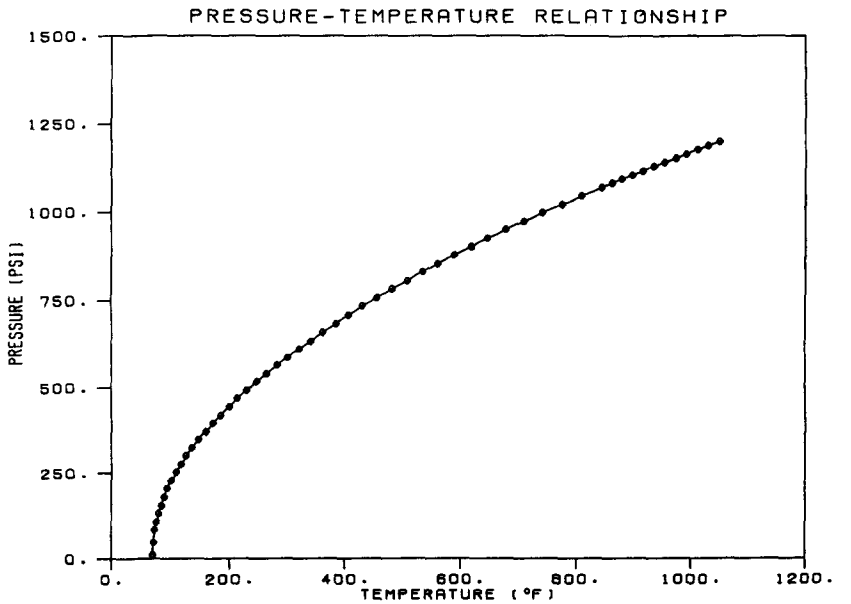

(b)

Fig. 6(a) Pressure vessel containing hot fluid—problem description; (b) Pressure–temperature relationship.

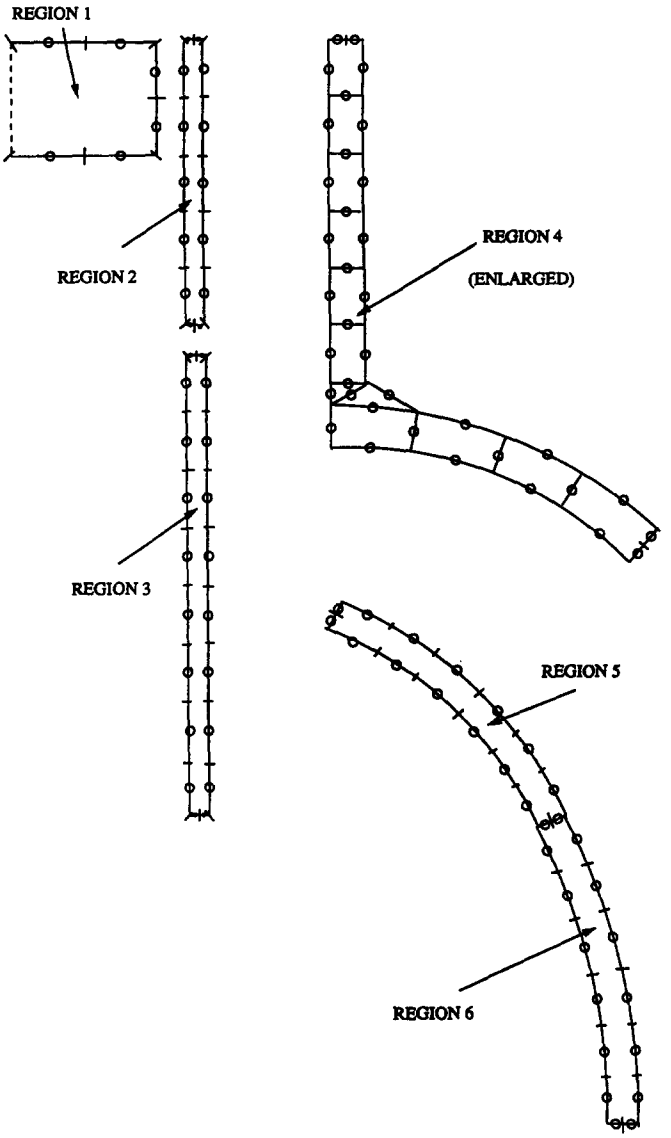

Fig. 7. Pressure vessel containing hot fluid—Boundary Element Model.

are in good agreement with the corresponding FEM results in Zienkiewicz (1977) for contours of plastic zones [refer inset of Fig. 8(b)]. It may be noted that the results obtained from the present analysis are very close to the results provided in Henry and Banerjee (1988) using BEM and consequently the latter are not plotted.

Next, the non-isothermal conditions are assumed and the fluid is considered to attain the two temperature states described earlier (i.e. 410°F and 632°F). The BEM results for the deflection of A with pressure and temperature are shown in Fig. 9 along with the corresponding isothermal case for comparison. It becomes evident that the increase in fluid temperature reduces the value of the collapse pressure significantly. The contours of the equivalent stress for the two pairs of pressure–temperature values are shown in the next figure. The isothermal distributions are plotted alongside for each case. For the first case, the effect of the thermal loading is seen to cause considerable change in the stress pattern [Fig. 10(a)]. This alteration of stress behavior becomes even more pronounced for the second case [Fig. 10(b)] where a much larger part of the wall develops very high stress values due to the additional thermal effects.

This problem emphasizes the enhanced ability of the present analysis to conduct realistic engineering studies of complex problems such as the one described above. It

(a)

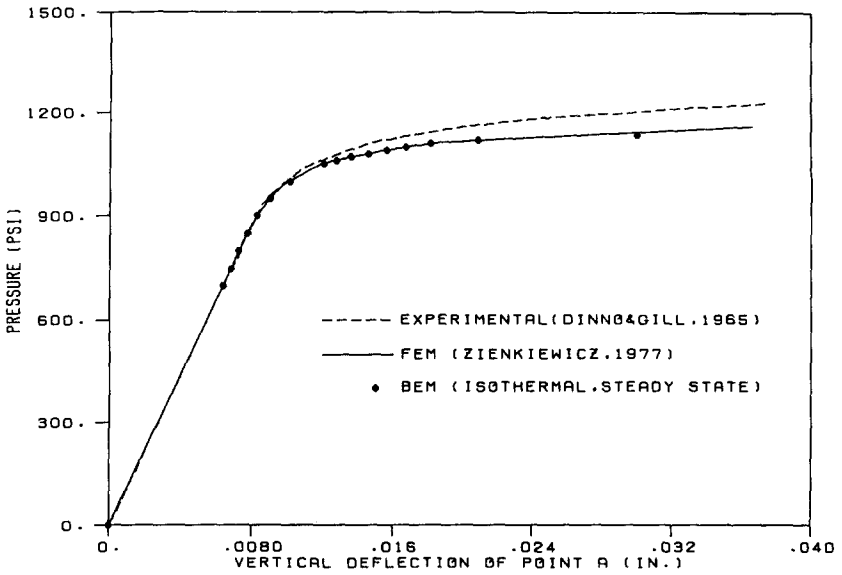

(b)

PROGRESS OF PLASTIC ZONE WITH INCREASING PRESSURE

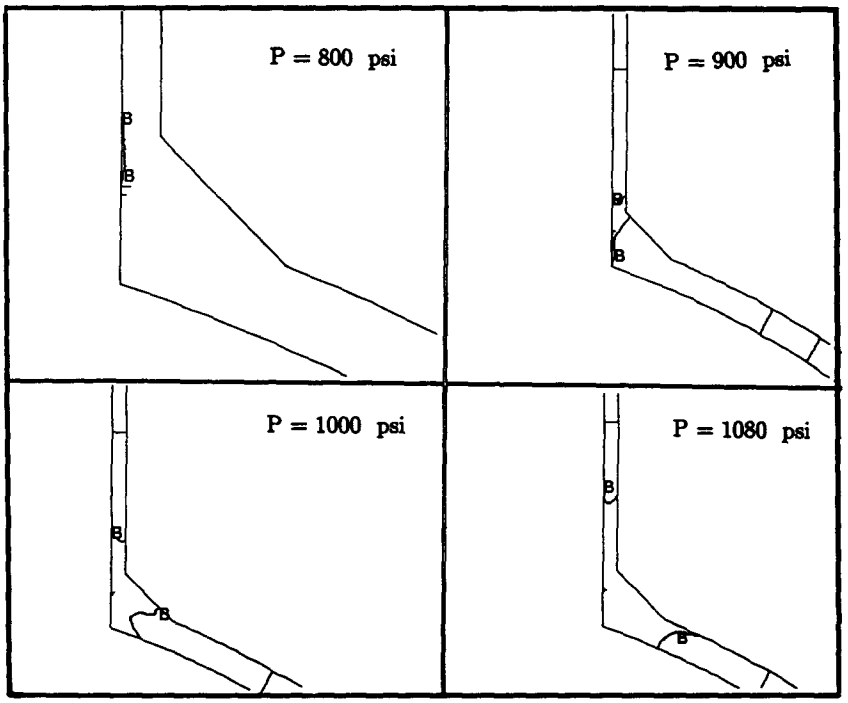

CONTOUR B : EQUIVALENT YIELD STRESS

Fig. 8(a) Vertical deflection of A as a function of the applied pressure—isothermal case; (b) Progress of yielded zones with increasing pressure.

provides confidence in using BEM for obtaining valuable information required for design and analysis of pressure vessels of any geometrical description.

(3) *Residual stresses in a cylindrical butt weld*

The measurement of residual stresses in the vicinity of butt-welded joints is a problem of considerable interest to engineers. In this section, the residual stresses in a cylindrical weld between two thin-walled, axisymmetric cylinders are studied.

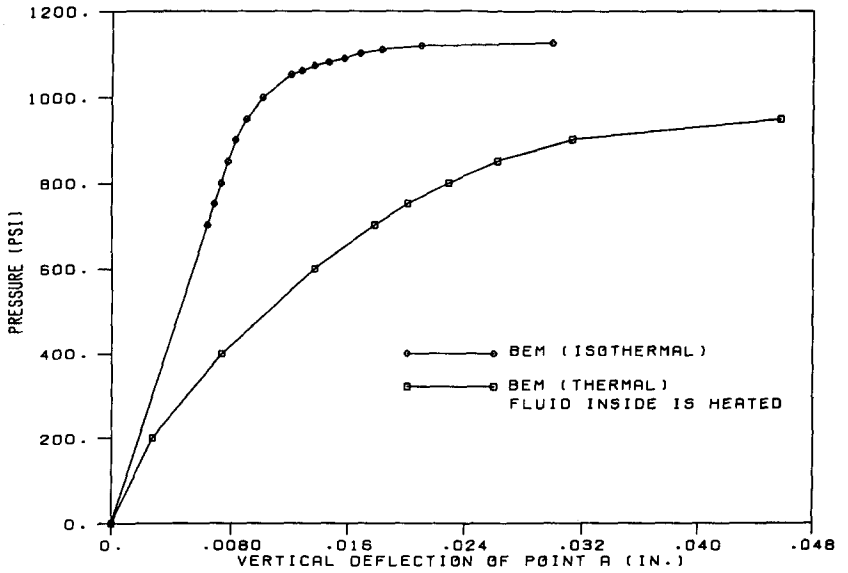

Fig. 9. Vertical deflection of A as a function of applied pressure and temperature.

In order to simplify the analysis, the cylinders and the weld are assumed to be completely stress-free until the completion of the pouring of the weld. The subsequent behavior as the weld is allowed to cool, is considered to be thermoplastic. This gives rise to residual stresses at the completion of the cooling. The far ends of the cylinders are permitted to deform freely.

The problem is described pictorially in Fig. 11. Two very long tubes are welded in the manner shown. The cross-sectional view of the assembly provides the details of the tube thickness and the weld geometry. For this hypothetical simulation, the outer diameter of the tube is selected as 3.0 in and the thickness as 0.5 in. A 45° weld is poured at the joint with a base of 0.1 in, as shown in Fig. 11. The material properties are chosen to be those of carbon steel and are listed below:

$$E = 29.0 \times 10^6 \text{ psi}$$

$$\nu = 0.3$$

$$\alpha = 6.0 \times 10^{-6} \text{ in(in °F)}^{-1}$$

$$\rho c_\varepsilon = 283.0 \text{ in} - \text{lb(in}^3 \text{ °F)}^{-1}$$

$$k = 5.8 \text{ in} - \text{lb(s in °F)}^{-1}.$$

A thermally-sensitive, two-surface model is employed for the nonlinear material behavior description. The inner yield stress is taken as $\sigma_y = 5$ ksi and the outer yield value is taken as $\sigma_y^b = 50$ ksi. The hardening modulus related to the bounding surface is $h^b = 10.0 \times 10^6$ psi and the material parameter $n = 4$ based upon a number of preliminary studies to simulate the hysteretic behavior of steel. The melting temperature of steel is taken as $T_{\text{melt}} = 2750$°F and initially, the weld is assumed to be close to this temperature. It should be noted at this juncture that the phase transformation from a liquid state to a solid state that precedes the cooling, is not simulated here. Only post-solidification cooling is considered with an assumption that the stress developed due to phase changes is not significant. The present formulation does not admit phase change phenomenon.

All surfaces are assumed to be convective in nature and a film coefficient of $h = 10.0$ in−lb (s in^2 °F)$^{-1}$ is selected. The outer surroundings are at room temperature (70°F). The axisymmetric BEM mesh employed for this problem is shown in Fig. 12. Utilizing symmetry about the midplane of the weld in the axial direction, only half of the weld and

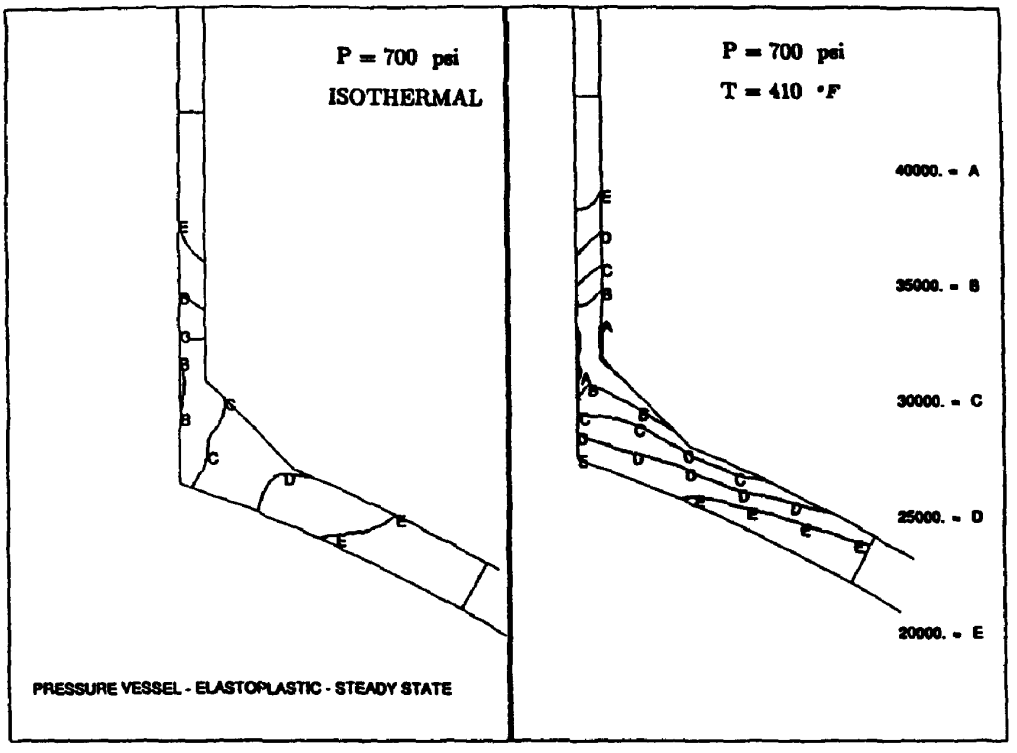

(a)

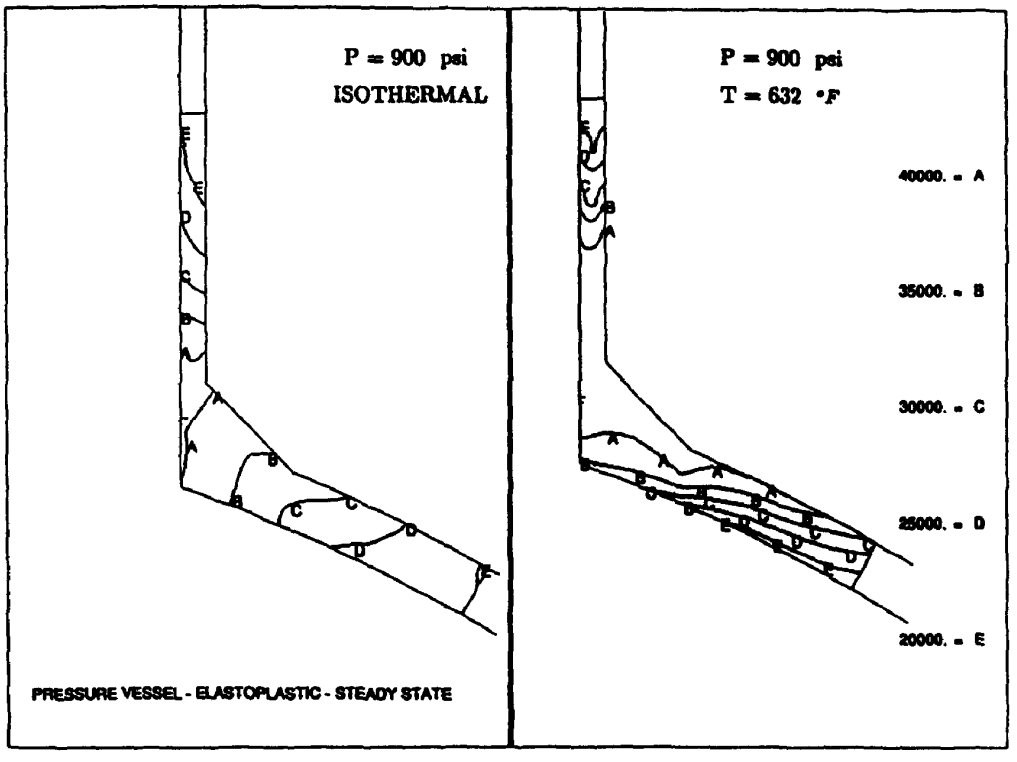

(b)

Fig. 10(a) Equivalent stress distribution at $P = 700$ psi for isothermal and thermal cases; (b) Equivalent stress distribution at $P = 900$ psi for isothermal and thermal cases.

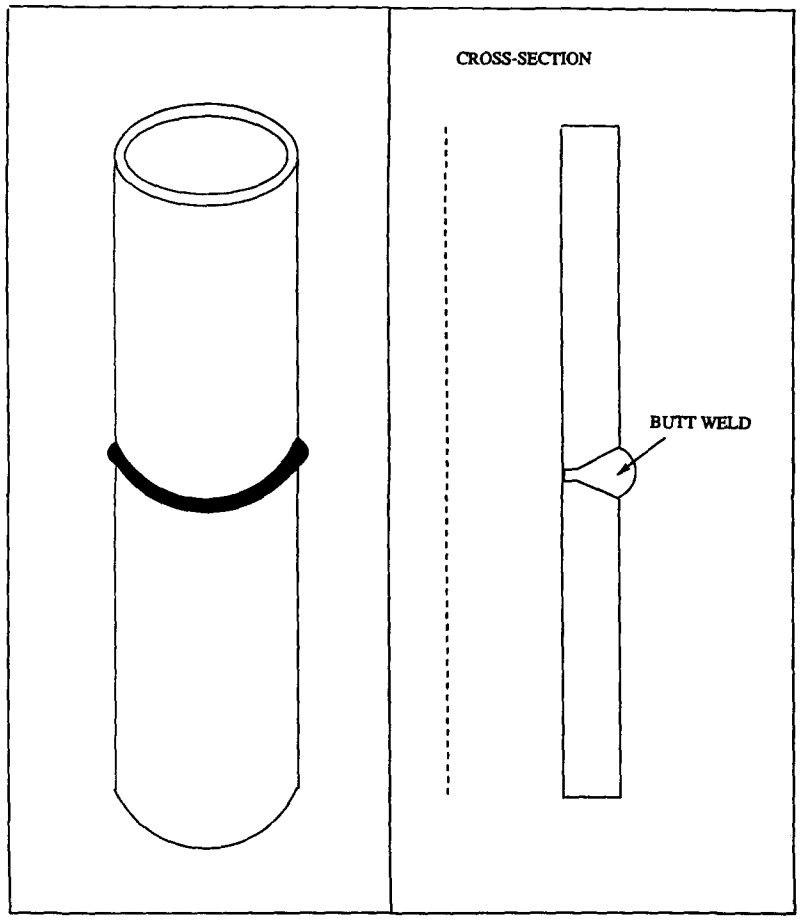

Fig. 11. Residual stress in a cylindrical butt weld—problem description.

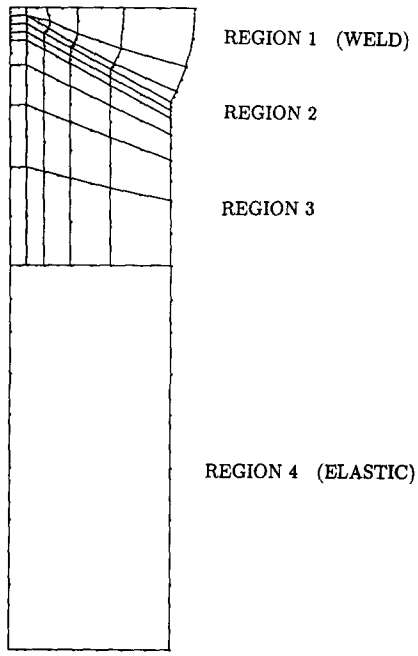

Fig. 12. Residual stress in a cylindrical butt weld—Boundary Element Model.

one of the tubes need to be modeled. The mesh is constructed of four regions, three of which are expected to yield. At a distance away from the weld, no yielding is anticipated and the fourth region is considered as elastic. The first region models the weld itself, using 15 quadratic boundary elements and 14 volume cells. This is followed by a thin zone of "pre-heating", which is commonly referred to as the heat affected zone (HAZ) (e.g. Karlsson, 1986). The initial temperature of this zone is assumed to have an intermediate value of 1035°F. Next to the HAZ lies the third region which is initially at room temperature but is expected to yield during the cooling process. It extends to about 1.6 times the thickness of the tube from the center of the weld.

A quasistatic analysis is carried out using the thermoplastic boundary element formulation. Based upon the element length and the diffusivity of the material, a time step of 0.04 s is selected. The first 8 s of the process is simulated and the temperature of the weld and the adjoining areas is found to be sufficiently low after this period.

Figure 13 shows the variation of temperature with time for the first 4 s at four different locations along the inner surface of the cylinder. The locations labeled 50 and 54 lie at the center and edge of the weld, respectively, and display a constant cooling trend from a very high initial value. The temperature of location 104 at the edge of the HAZ initially rises and then decays. Lastly, the location 186, which is the furthest from the weld, displays only a small variation from initial room temperature.

The deflected shape of the welded cylinder is shown in Fig. 14 at the completion of 8.0 s of cooling. Since the radial movement of the cylinder is unrestrained, it bends inwards as the weld cools and shrinks. This takes place to minimize the total strain energy by relieving the hoop stress in the weld. As a result, significant axial stress build-up is observed from the differential radial displacements.

The residual axial and hoop stress variation at the end of 8.0 s along the axial coordinate from the center of the weld at the inner surface of the tube, is plotted in Fig. 15. The hoop stress is tensile around the welded zone and becomes compressive away from the edge of the weld. On the other hand, the axial stress is compressive in the weld, becomes tensile in the immediate vicinity (at the interface) and then compressive again away from the edge of the weld. This is due to the large thermal gradient between the weld and the adjoining region. This agrees well with the observations made in fracture studies of cylindrical welds (Vaidyanathan *et al.*, 1973). Cracks in cylindrical specimens are noticed to be initiated in the axial direction and then turn into the circumferential direction. Assuming that a crack grows in a way that keeps its plane perpendicular to the plane of maximum tensile stress, the predicted results agree well with such observations.

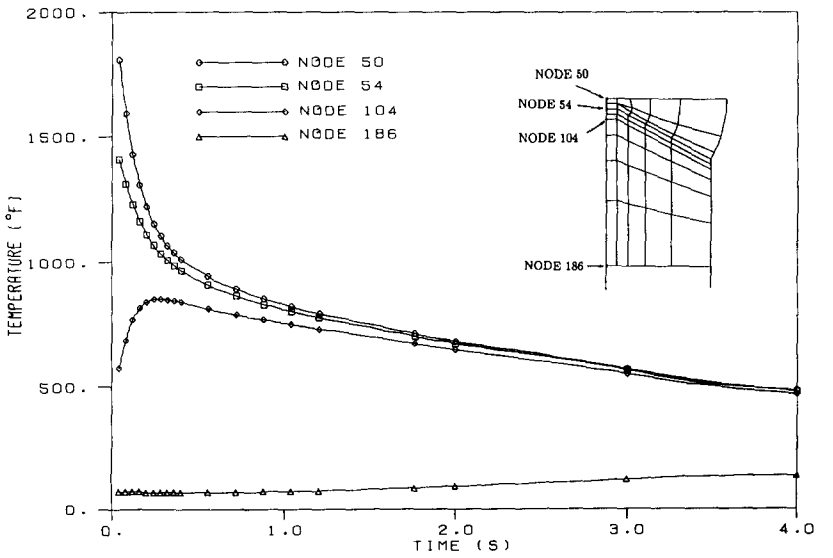

Fig. 13. Temperature variation with time at four locations.

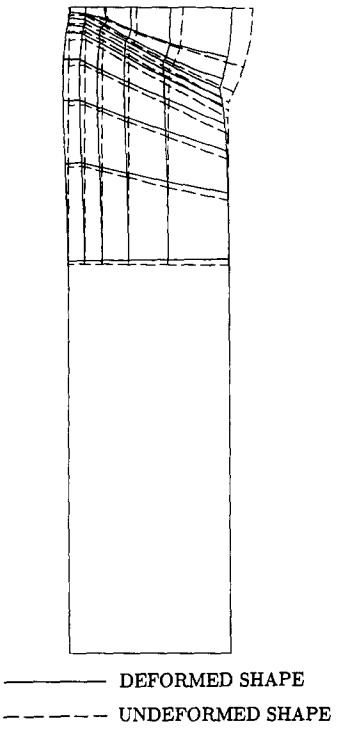

Fig. 14. Deformed shape at the end of 8.0 s of cooling.

A simplified and idealized simulation of the development of thermal stresses due to the cooling of a cylindrical weld has been briefly discussed above. (More details concerning the simulation can be found in Chopra, 1991.) In reality, the process is more complex involving several different stages, each of which may give rise to stresses in the cylinder. In the future, advanced features, such as moving boundary conditions and sources, time-dependent material properties and variable time-stepping may be incorporated within the present development to conduct a more realistic simulation of the welding process.

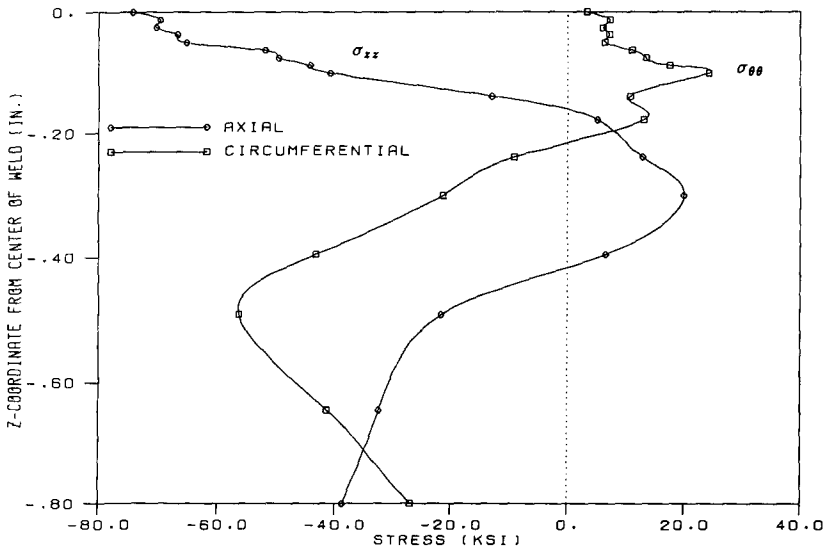

Fig. 15. Residual axial and circumferential stress along axial coordinate from the center of the weld.

CONCLUSIONS

An advanced boundary element method has been developed for general thermoplastic analysis. The formulation includes the use of a thermally-sensitive two-surface constitutive model and a Newton–Raphson solution algorithm. This permits the application of BEM to a range of physical problems involving thermomechanical processing and operation. Several representative applications were presented in detail.

However, much additional work is still required to elevate the current BEM approach to the same level currently attained by FEM. Thermo-viscoplastic material models are necessary in order to accommodate creep phenomena, and the effects of finite deformation must be incorporated into the formulation. From the algorithmic side, analytic formulae must be developed for all of the volume integrals, and a substructured solution strategy is needed. Based upon the experience gained to-date, the authors believe that the resulting BEM will be worth the effort, particularly for complex three dimensional thermoplastic problems.

REFERENCES

Banerjee, P. K. and Butterfield, R. (1981). *Boundary Element Methods in Engineering Science*. McGraw-Hill, London.

Banerjee, P. K. and Raveendra, S. T. (1986). Advanced boundary element of two- and three-dimensional problems of elastoplasticity. *Int. J. Numer. Meth. Engng* **23,** 985–1002.

Banerjee, P. K. and Raveendra, S. T. (1987). A new boundary element formulation for two-dimensional elasto-plastic analysis. *J. Engng Mech., ASCE* **113,** 252–265.

Banerjee, P. K., Wilson, R. B. and Raveendra, S. T. (1987). Advanced applications of BEM to three-dimensional problems of monotonic and cyclic plasticity. *Int. J. Mech. Sci.* **29**(9), 637–653.

Boley, B. A. and Weiner, J. H. (1960). *Theory of Thermal Stresses*. Wiley, New York.

Chopra, M. B. (1991). Linear and nonlinear analyses of axisymmetric problems in thermomechanics and soil consolidation, Ph.D. Dissertation, State University of New York at Buffalo.

Dafalias, Y. F. and Popov, E. P. (1974). A model of nonlinearly hardening material for complex loading. *Proc. 7th U.S. National Congress in Appl. Mech. Boulder, Acta Mech.* 21, 173–192.

Dargush, G. F. and Banerjee, P. K. (1989). The boundary element method for plane problems of thermoelasticity. *Int. J. Solids Structures* **25,** 999–1021.

Dargush, G. F. and Banerjee, P. K. (1990). BEM analysis for three-dimensional problems of transient thermo-elasticity. *Int. J. Solids Structures* **26,** 199–216.

Dargush, G. F. and Banerjee, P. K. (1991). Boundary element methods for three-dimensional thermoplasticity. *Int. J. Solids Structures* **28**(5), 549–565.

Dinno, K. S. and Gill, S. S. (1965). An experimental investigation into the plastic behavior of flush nozzles in spherical pressure vessels. *Int. J. Mech. Sci.* **7,** 817–835.

Henry, D. P. and Banerjee, P. K. (1988). A thermoplastic BEM analysis of substructured axisymmetric bodies. *J. Engng Mech., ASCE* **113**(12), 1880–1900.

Karlsson, L. (1986). Thermal stresses in welding. In *Thermal Stresses I* (Edited by R. B. Hetnarski). Elsevier Science Publishers, B.V.

Krieg, R. D. (1975). A practical two surface plasticity theory. *J. Appl. Mech., ASME* **E42,** 641–646.

Mröz, Z. (1967). On the description of anisotropic work hardening. *J. Mech. Phys. Solids* **15,** 163–175.

Mustoe, G. G. W. (1984). Advanced integration schemes over boundary elements and volume cells for two- and three-dimensional nonlinear analysis. In *Developments in Boundary Element Methods—III* (Edited by P. K. Banerjee and S. Mukherjee). Applied Science Publishers, England.

Vaidyanathan, S., Todaro, A. F. and Finnie, I. (1973). Residual stresses due to circumferential welds. *J. Engng Materials Technology, ASME*, 233–237.

Zienkiewicz, O. C. (1977). *The Finite Element Method*, Third Edition. McGraw-Hill, London.